Structure of monolayer tin oxide films on Pt (111) formed using NO_{2} as an efficient oxidant

Article *in* Physical Review B · November 2001

DOI: 10.1103/PhysRevB.64.245402

3 authors:

Matthias Batzill
University of South Florida
153 PUBLICATIONS **9,564** CITATIONS
SEE PROFILE

David Beck
Oxford Instruments Asylum Research Inc.
16 PUBLICATIONS **261** CITATIONS
SEE PROFILE

Bruce Koel
Princeton University
377 PUBLICATIONS **12,787** CITATIONS
SEE PROFILE

Structure of monolayer tin oxide films on Pt(111) formed using NO_2 as an efficient oxidant

Matthias Batzill, David E. Beck, and Bruce E. Koel*
Department of Chemistry, University of Southern California, Los Angeles, California 90089-0482
(Received 3 May 2001; revised manuscript received 7 August 2001; published 20 November 2001)

Submonolayer Sn deposits on Pt(111) and Sn incorporated in a $(\sqrt{3}\times\sqrt{3})R30°$ Sn/Pt(111) surface alloy were oxidized by NO_2 under ultrahigh-vacuum conditions. The oxide films formed were characterized by Auger-electron spectroscopy, low-energy electron diffraction (LEED), and scanning tunneling microscopy (STM). Four different surface morphologies were identified, depending on the preparation conditions, each of them exhibiting a distinct LEED pattern. STM revealed two ordered epitaxial overlayers. One is interpreted as the adsorption of SnO pseudomolecules at preferential sites to form a (4×4) coincidence lattice with the substrate. The other structure forms an incommensurate tin oxide overlayer, exhibiting a long-range Moiré pattern. The remaining LEED patterns are associated with the formation of a regular stress-relief pattern that can transform into an ordered array of tin oxide islands upon repeated oxidation. This ordered island array exhibited a (5×5) superlattice with respect to the Pt(111) substrate. The variety of SnO_x overlayer morphologies is attributed to subtle differences in the oxide stoichiometry and alterations in the oxide/metal interface, in particular Pt-Sn alloying.

DOI: 10.1103/PhysRevB.64.245402 PACS number(s): 68.35.−p, 81.65.Mq, 68.55.Jk

I. INTRODUCTION

Ultrathin oxide films on single-crystal metal supports have been studied in the past to create model systems for bulk oxide surfaces. Such oxide films often allow for electron transport that is essential for scanning tunneling microscopy (STM) studies and may improve the performance of standard surface science probes.[1,2] Although it has been shown that some of these surfaces are useful substitutions for bulk oxide surfaces and are often used as supports for creating nanodispersed metal catalysts in research laboratories,[3–9] there is also compelling evidence that these ultrathin oxide films possess altered properties and structures compared to bulk oxide surfaces. This is partly due to their low dimensionality, but mainly it is a result of the oxide interaction with the support. As a consequence, ultrathin oxide films can be grown that are not thermodynamically stable as bulk materials. One such example is the growth of FeO on Pt(111).[10–14] Some of these novel materials exhibit unique electronic[15,16] and/or ferromagnetic properties.[17] Furthermore, bulk oxides often lack stable polar surfaces, but these surfaces may also be stabilized on ultrathin films.[18] In this article it is shown that more than one tin oxide (SnO_x) ultrathin film is stable on a Pt(111) substrate. This illustrates at once the complexity of oxide/metal interfaces and their potential for developing novel surfaces with unique structures and properties.

In order to put the formation of SnO_x layers on Pt(111) in context, studies of other ultrathin oxide films on Pt(111) can be cited. Oxidation studies of Ce (Ref. 19), Al (Ref. 16), Cr (Refs. 20 and 17), and Fe (Refs. 10–14) on Pt(111) have been presented previously. For all of these systems, the formation of an ordered overlayer was reported following annealing of the sample. Specifically, the formation of tin oxide layers on Au(111) (Ref. 21) and Pd(111) (Ref. 15) has been studied previously. Oxidizing a tin overlayer on gold and subsequent annealing did not produce an ordered oxide layer, but it was reported that oxidation at elevated temperatures (500–800 K) formed an ordered, SnO_2 overlayer on gold. However, at least one-half of the tin in the adlayer diffused into the gold crystal under these conditions. The oxidation of a Sn overlayer on Pd(111) is of particular relevance to this study, because the Pd/Sn bimetallic system behaves similarly to Pt/Sn with respect to the formation of stable surface alloys.[22] It was concluded that submonolayer amounts of Sn can be oxidized to a SnO stoichiometry on Pd(111). Furthermore, the thermal stability of these oxide layers was markedly less than that for bulk Sn oxide, and it was suggested that exothermic Pd/Sn alloying may promote the redox chemistry of tin oxide films.

Motivation for the study of the tin oxide/Pt and Pt-Sn alloy interfaces is the important role played by such interfaces in practical or technical systems. For instance, bimetallic Pt-Sn catalysts are used in hydrocarbon reforming[23–26] and Pt-Sn alloys are active phases in a number of existing and developing catalysts.[27–31] Furthermore, Pt particles on tin oxide supports are used as catalysts for CO oxidation.[32] SnO_2 is also a widely used material for sensing toxic gases[33–36] such as Co, NO_2, and O_3. In these gas-sensing devices, Pt is sometimes used as a promoter. For all of the applications given above, it is anticipated that a basic understanding of the SnO_x/Pt interface should enable improvements to be made in practical systems.

Oxidation of the (2×2) and $(\sqrt{3}\times\sqrt{3})R30°$ Sn/Pt(111) surface alloys using NO_2 (Ref. 37) and O_3 (Ref. 38) as oxidants under ultrahigh-vacuum (UHV) conditions has been studied previously in our group. Surprisingly, the thermal stability of the oxide films for the two oxidized surface alloys were found to be significantly different. The SnO_x layer that formed by oxidizing the (2×2) alloy is unstable above 800 K, while the oxide layer for the oxidized $(\sqrt{3}\times\sqrt{3})R30°$ surface alloy does not decompose below 1000 K. Furthermore, the oxidized $(\sqrt{3}\times\sqrt{3})R30°$ surface alloy exhibits ordered surface structures upon annealing to 900 K. O_2 desorption curves in temperature-programmed desorption

showed two peaks for the oxidized $(\sqrt{3}\times\sqrt{3})R30°$ Sn/Pt(111) surface alloy. The first and larger peak at around 800 K was associated with oxygen desorbing from Pt sites and the second peak at 1000 K was affiliated with the decomposition of a tin oxide adlayer. The oxygen concentration in the tin oxide film was estimated to be between 0.1 and 0.15 monolayer (ML).[38] It was proposed that dosing O_3 or NO_2 caused the extraction of tin out of the Sn/Pt surface alloy to form a tin oxide adlayer. X-ray photoelectron spectroscopy (XPS) studies of the oxidation of the $(\sqrt{3}\times\sqrt{3})R30°$ Sn/Pt(111) surface alloy showed a broadening of the Sn($3d$) lines.[37] These Sn peaks were deconvoluted into three Sn states, a Sn^0 state from alloyed Sn and two states shifted in binding energy by $\Delta E_B = 0.6$ and 1.6 eV. However, no shift large enough to be associated with a fully oxidized Sn^{4+} state was observed, i.e., no SnO_2 was present. Sn is only present in reduced oxidation states such as Sn^{1+} or Sn^{2+}. XPS studies also showed that a structural change observed by low-energy electron diffraction (LEED) between 840 and 1000 K, as described in more detail below, is accompanied by an increase of the Sn^0 component without changing the oxidized Sn components significantly. This was explained by a small amount of Sn segregation from the bulk to the surface.

In this article, LEED and STM data are used to characterize the SnO_x adlayers formed by oxidation of a $(\sqrt{3}\times\sqrt{3})R30°$ Sn/Pt(111) surface alloy and several Sn overlayers on Pt(111). For the purpose of this article, the more thermally stable oxide films formed on these surfaces rather than those on the oxidized (2×2) Sn/Pt(111) surface alloy were studied. Such tin oxide adlayers exhibit several possible overlayer structures depending on the preparation conditions.

II. EXPERIMENTAL METHODS

Experiments were performed in an UHV chamber equipped with a cylindrical mirror analyzer for Auger-electron spectroscopy (AES), rear-view LEED optics, a quadrupole mass spectrometer for residual gas analysis and temperature-programmed desorption (TPD), a home-built single-piezotube STM, an ion gun for sample cleaning, a resistively heated, Sn-evaporation source, and precision leak valves for gas dosing, including one directed-beam gas doser for NO_2 exposures. For AES, the electron gun and energy analyzer were positioned normal to the sample surface. The incident-electron energy was 3 keV and the modulation voltage used to record the spectra in $dN(E)/dE$ mode was 6 eV. The sample was heated by electron-beam heating from the backside of the single crystal, and the sample temperature was measured by a chromel/alumel thermocouple spot welded directly to the side of the crystal.

The Pt(111) single crystal was cleaned by standard procedures, consisting of cycles of 500-eV Ar^+-ion sputtering, annealing at 1000 K in 2×10^{-7} Torr O_2, and finally annealing at 1200 K in UHV. The cleanliness of the sample was monitored by AES. The Sn deposition rate was calibrated by means of AES uptake plots. From the uptake plots a deposition rate of 0.01 ML/sec was estimated, which was kept constant for all experiments. The tin coverage after every deposition of tin was confirmed by measuring the Sn(430 eV) to Pt(237 eV) peak-to-peak ratio in the AES spectrum. To form the $(\sqrt{3}\times\sqrt{3})R30°$ Sn/Pt(111) surface alloy, ~1.0 ML Sn was deposited at 300 K on the Pt(111) crystal and subsequently annealed to 1000 K for 10 s.[39] This caused the Sn/Pt AES ratio to decrease from 7.8 to 2.5.

In order to oxidize the $(\sqrt{3}\times\sqrt{3})R30°$ surface alloy or Sn adlayers under UHV conditions, NO_2 was dosed for 40 s at a background pressure of 4×10^{-8} Torr with the sample temperature held at 400 K. This temperature was chosen to avoid NO adsorption on the surface. In reporting the NO_2 exposures, no account was taken for the ion-gauge sensitivity or enhancement factor for the directed gas doser. TPD showed that the NO_2 exposures used resulted in a saturation of the surface with oxygen. No nitrogen contamination of the samples was detected by AES.

III. RESULTS

Two different kinds of samples were investigated: (i) $(\sqrt{3}\times\sqrt{3})R30°$ surface alloys containing Sn incorporated into the surface plane with $\Theta_{Sn}=0.33$, and (ii) 0.4-ML coverage of Sn adatoms on the Pt(111) surface. After saturating the surface with oxygen by exposure to NO_2, the samples were flash-annealed to several target temperatures and the resulting surfaces were characterized by AES, LEED, and STM. The resulting surface structures are presented in the next two sections. Repeated oxidation and annealing cycles resulted in different surface morphologies, and the surface structures formed in this manner are presented in the third following section.

A. Oxidation of a $(\sqrt{3}\times\sqrt{3})R30°$ Sn/Pt(111) surface alloy

Exposure of NO_2 on a $(\sqrt{3}\times\sqrt{3})R30°$ alloy at 400 K causes oxygen uptake and the appearance of an oxygen peak in AES. Such oxidized samples were flash-annealed to several target temperatures and were characterized by AES, LEED, and STM after cooling down to room temperature.

The evolution of the surface composition with annealing temperature as recorded by AES is shown in Fig. 1. The O(510 eV)/Sn(430 eV) and O(510 eV)/Pt(237 eV) peak-to-peak ratios in AES [Fig. 1(b)] showed a behavior consistent with that reported previously for the oxidation of the same surface alloy with ozone.[38] Most of the oxygen desorbed from the surface upon annealing to 860 K. The O(510 eV)/Sn(430 eV) ratio for the oxidized $(\sqrt{3}\times\sqrt{3})R30°$ alloy did not change significantly in the temperature range between 860 and 1020 K. At 1020 K, the tin oxide film decomposed and oxygen desorbed from the surface. Further annealing to 1060 K caused the oxygen peak in AES to vanish.

Dosing NO_2 at 400 K on the $(\sqrt{3}\times\sqrt{3})R30°$ surface alloy resulted in a diffuse LEED image with no diffraction spots. The first-order, Pt(111) substrate spots only appeared upon annealing the sample to 600 K, but there was still a diffuse background with no additional apparent ordering of the surface. Further annealing to 830 K resulted in a complex LEED pattern of diffuse spots as shown in Fig. 2(a). However, flash annealing of the sample to 860–880 K gave a

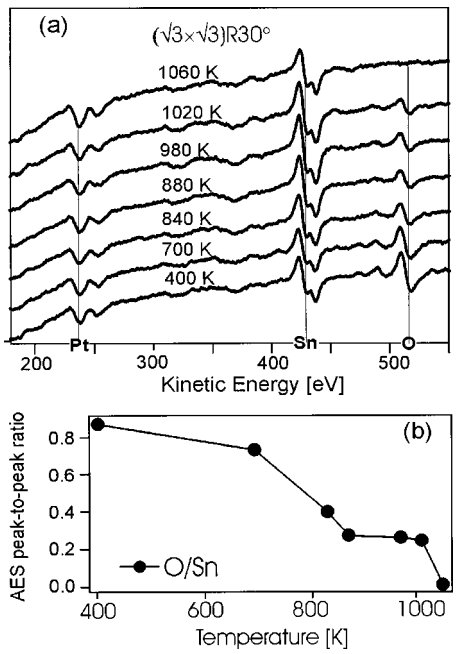

FIG. 1. (a) AES spectra taken at successive annealing temperatures for a $(\sqrt{3}\times\sqrt{3})R30°$ Sn/Pt(111) surface alloy exposed to a saturation dose of NO_2. (b) Plot of AES peak-to-peak ratios for the O(510 eV) and Sn(430 eV) peaks. After initial desorption of oxygen from the oxidized surface below 880 K, the O/Sn ratio does not change significantly over the temperature range between 880 and 1020 K.

clear LEED pattern, which is shown in Fig. 2(b). This structure is called ''structure I'' in the following discussion. Annealing further to 900–1000 K, or annealing to 850 K for several minutes, resulted in the appearance of a (4×4) LEED pattern shown in Fig. 2(c). STM images that were obtained for the latter two surfaces are displayed in Fig. 3.

As shown in Fig. 3(a), STM images of structure I, associated with the lower annealing temperature (860–880 K), exhibits areas with rows oriented along the $\langle\bar{1}01\rangle$ direction. The width of the rows coincides with 5 times the separation between Pt rows in the $\langle\bar{1}10\rangle$ direction on the Pt(111) substrate. Three domains, with rows orientated at 60° with respect to each other, were observed. Large undulations within these rows are visible in the STM images. These undulations appear to have a minimum separation of 5 times the Pt(111) surface-lattice constant along the rows and in general are separated by a multiple thereof. Neighboring undulations on adjacent rows appear to preferentially form a 60° angle with respect to the row orientation.

Samples that were annealed to 900–1000 K and exhibited the (4×4) LEED pattern showed ordered regions in the STM images [Figs. 3(b) and 3(c)] from which a (4×4) unit cell can be constructed. Rows of protrusions with a periodicity of 2 times the Pt(111) surface lattice constant were observed. These rows occur in all three equivalent symmetry directions of the (111) surface, and are separated by four surface lattice constants. This gives rise to the (4×4) LEED pattern [see Figs. 3(c) and 3(d)]. The corrugation of these protrusions is between 0.08 and 0.12 nm. STM images also show that many vacancies and other defects exist in the (4×4) superstructure.

For completeness, we mention in this context that recent experiments on the growth of Sn oxide multilayer films on Pt(111) found that growth proceeds via a Stranski-Krastanov mode with the wetting layer generally exhibiting the same (4×4) structure as described above. However, (4×6) and (4×8) domains were also identified by STM. These structures were never encountered on the oxidized surface alloys or oxidized submonolayer-Sn deposits described in this article. Therefore, we will leave a more detailed discussion of these structures for a forthcoming article on the multilayer growth of Sn oxide films.[40]

Annealing of these surfaces to 1200 K resulted in the complete decomposition of SnO_x species and desorption of all surface oxygen. LEED and STM showed that such a reduced surface reorders into a (2×2) Sn/Pt(111) surface alloy.

B. Oxidation of tin overlayers

A submonolayer-Sn film was deposited on Pt(111) at 300 K. This forms tin islands in the adlayer. Oxidation of the Sn overlayer was performed by using NO_2 and the same procedure as above.

Oxidation of a Sn adlayer with 0.4-ML Sn coverage and subsequent annealing to 860–950 K yielded surfaces that exhibited the same (4×4) LEED pattern as formed after oxidizing the $(\sqrt{3}\times\sqrt{3})R30°$ alloy. However, the intermedi-

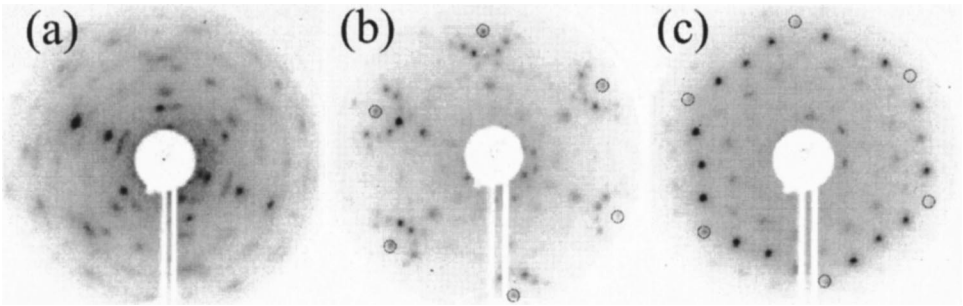

FIG. 2. LEED patterns for the evolution of an oxidized $(\sqrt{3}\times\sqrt{3})R30°$ Sn/Pt(111) surface alloy after annealing to (a) 840 K (incident beam energy, $E_p=77$ eV), (b) 880 K ($E_p=70$ eV), and (c) 920 K ($E_p=77$ eV). The first-order spots of the Pt(111) substrate are marked by circles in (b) and (c). Image (b) shows a LEED pattern that corresponds to structure I on the surface and (c) exhibits a clear (4×4) pattern.

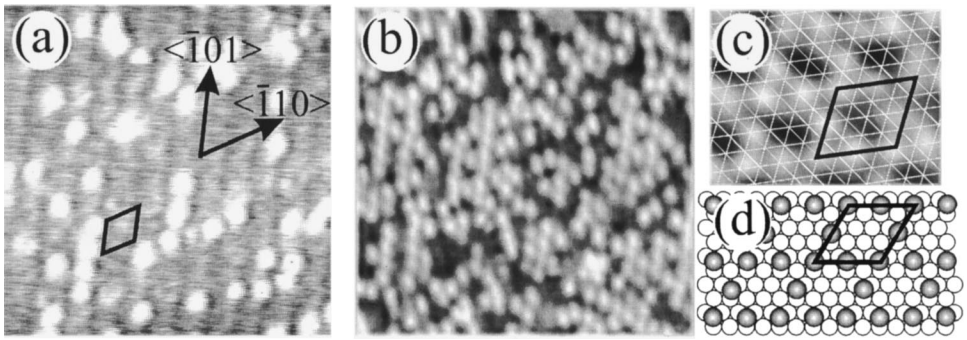

FIG. 3. (a) STM image ($20\times20\,\mathrm{nm}^2$, $U_{\mathrm{bias}}=150\,\mathrm{mV}$, $I=0.2\,\mathrm{nA}$) of structure I on the surface obtained after annealing to 880 K. A row structure is visible with protrusions within the rows. A (5×5) unit cell is shown that describes the $5a_{\mathrm{Pt}}$ spacing of the rows and the minimum separation between the protrusions both along the rows and on neighboring rows. (b) STM image ($12\times12\,\mathrm{nm}^2$, $U_{\mathrm{bias}}=150\,\mathrm{mV}$, $I=0.3\,\mathrm{nA}$) of a (4×4) surface obtained after annealing to 920 K. Rows of protrusions with twice the Pt-lattice spacing in all three low-index directions of the substrate can be identified, although a high density of ''missing'' protrusions is apparent. (c) Small scan area of a well-ordered (4×4) structure. The white lines represent the Pt(111) lattice and the black line shows the (4×4) unit cell. (d) Schematic model for the (4×4) structure in which shaded circles indicate SnO pseudomolecules. Open circles show the Pt(111) substrate. The adsorption sites on the surface are unknown and thus the registry of the shaded circles for the adlayer with respect to the open circles of the substrate is arbitrary.

ate structure, i.e., structure I, that was found to exist over a narrow temperature window for the oxidized and flash-annealed $(\sqrt{3}\times\sqrt{3})R30°$ surface alloys was never observed by oxidizing Sn overlayers.

C. Repeated NO_2 dosing

After having obtained the (4×4) structure, either by oxidizing and subsequently annealing the $(\sqrt{3}\times\sqrt{3})R30°$ alloy or a 0.4-ML-thick Sn overlayer, we exposed this surface to NO_2 again, repeatedly, in order to determine if the surface was completely oxidized or if additional oxygen could be added to the surface. We followed the same procedure for repeated oxidation treatments as for the initial oxidation step. After annealing the surface to 860 K, structure I was observed most frequently on the surface. However, now this structure was stable up to 1000 K. The (4×4) structure did not form. The situation is quite complex since a different surface structure, which we call ''structure II'' in the following discussion, was obtained occasionally after the second NO_2 exposure. Structure II was never observed after the first NO_2 exposure. This structure is characterized by a complex LEED pattern and an ordered overlayer structure in STM images as shown in Fig. 4. The formation of structure II appeared to be independent of the history of the sample, i.e., it did not matter if one started with the $(\sqrt{3}\times\sqrt{3})R30°$ alloy or a Sn adlayer. A considerable amount of time attempting to identify reliable procedures to reproduce surfaces with either structure I or II was spent; however, the parameters responsible for guaranteeing the formation of one or the other surface could not be determined. Structure I was the more commonly observed surface structure.

Although there was no significant difference in the O(510 eV)/Sn(430 eV) AES ratios between structures I and II, the two surfaces have very different structural features. This is manifested in the STM images and LEED patterns from both surfaces [Figs. 2(b), 3(a), and 4]. Structure I is much less ordered, although it exhibits regularly spaced rows. No atomic-resolution STM images on structure I surfaces were obtained. Both structures exhibit three rotational domains that can be imaged by STM. Individual domains are rotated by 60° with respect to each other [e.g., see Fig. 4(c) for structure II]. Structure II is more ordered, and no irregularly spaced protrusions could be identified. STM images showed that the domain boundaries of structure II were decorated with material [Fig. 4(c)]. Such a decoration of domains was not observed for structure I. Figure 4(b) shows that a long-range surface modulation could be observed in the STM images. Such a Moiré pattern indicates that there is an incommensurate SnO_x film on the Pt(111) substrate. However, ordering into three rotational domains indicates that there is a fixed orientational relationship between the oxide film and the Pt(111) substrate. By combining the information from high-resolution STM images, observation of the Moiré pattern, and the LEED pattern, it is obvious that structure II represents an ordered tin-oxide film on the Pt(111) substrate.

Tip changes were observed sometimes that significantly changed the corrugation in the STM images. Such changes are shown in Fig. 4(d). These abrupt changes were most likely due to a ''pick-up and drop'' mechanism of an adsorbate by the STM tip. This significantly changes the tunneling characteristics between the tip and surface. In Fig. 4(d) one can see that in addition to increasing the corrugation when an adsorbate is picked up by the tip, the contrast is reversed also, i.e., rows that were imaged as depressions without an adsorbate at the tip are imaged as protrusions with an adsorbate at the tip. Such a change in contrast and corrugation indicates that the adsorbate interacts with different parts of the surface pattern differently. This provides strong support for interpreting the rows as not only arising from topographical variations, but that the chemical termination of the surface is different at regions on top of the rows and between the rows.

High-resolution STM images of structure II could be readily achieved. From these images, a unit cell can be con-

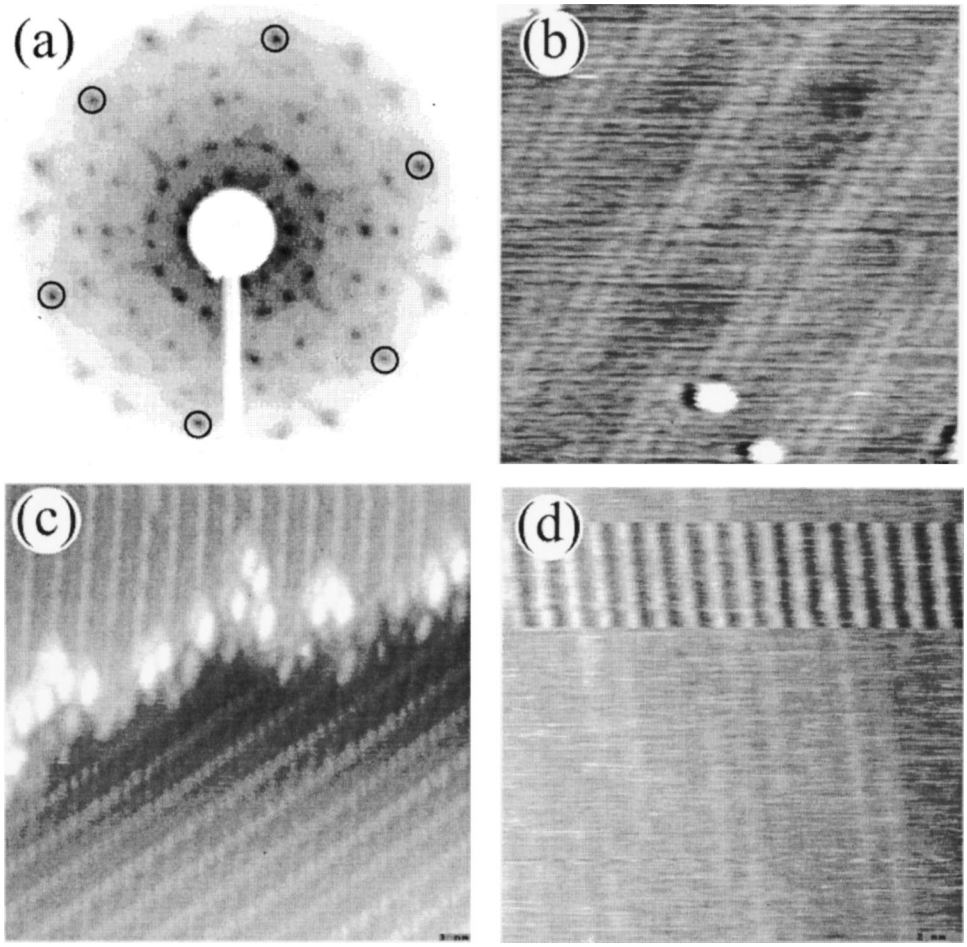

FIG. 4. (a) LEED pattern of structure II on the surface. The first-order spots of the Pt(111) surface are marked by circles ($E_p = 77$ eV). (b), (c), and (d) are STM images of this surface. (b) A Moiré pattern can be identified (scan area: 18×18 nm^2, $U_{\text{bias}}=200$ mV, $I=0.2$ nA). (c) Two domains separated by a terrace step. The domains are rotated by 60°. Decoration of the domain boundaries with material was always observed. The image size is 15×15 nm^2 ($U_{\text{bias}}=100$ mV, $I=0.3$ nA). (d) The tunneling tip changed its tunneling characteristics by ''picking up'' an adsorbate and depositing it again. The measured corrugation increased significantly by picking up the adsorbate, suggesting a variation of the adsorbate-surface interaction with different parts of the surface pattern. The image size is 15×15 nm^2 ($U_{\text{bias}}=150$ mV, $I=0.2$ nA).

structed that agrees with the LEED pattern [Figs. 5(a)–5(c)]. The unit cell deduced from LEED and STM is a parallelogram with a size of 1.09×0.61 nm. The directions of the sides of the parallelogram are rotated with respect to the Pt $\langle110\rangle$ directions by 10° and 18°, respectively. On occasion, additional LEED spots were found that suggest commensurate structures in the Sn oxide adlayer. The unit cell constructed from these additional LEED spots is a rectangular superstructure that can be expressed in matrix notation as $\left(\begin{smallmatrix}2 & 0\\ 1 & 2\end{smallmatrix}\right)$ as shown in Fig. 5(d). STM images of these surfaces reveal areas that exhibit high densities of defects or larger separations between the otherwise characteristic rows on the surface. Between the rows with increased separation, or areas between ''fragmented rows,'' a rectangular structure can be identified in the STM images as shown in Fig. 5(e). The length of the rectangular unit cell in the STM images corresponds closely to that of the corresponding unit cell observed in LEED.

Continued oxidation-treatment cycles by repeated NO_2 dosing and annealing of structure I eventually resulted in a clear (5×5) LEED pattern as shown in Fig. 6(a).[41] The number of oxidation steps necessary to obtain such a structure varied between three and five. STM images revealed a surface that was covered with tiny islands on top of extended terraces that are formed by atomic steps on the Pt(111) crystal. These islands were ordered on a (5×5) grid with respect to the Pt(111) substrate as shown in Figs. 6(b) and 6(d). The islands were of irregular shape and separated by narrow gaps that are apparently 0.1–0.2 nm in depth as shown in Fig. 6(c).

IV. DISCUSSION

There is no single structure that characterizes ultrathin tin oxide films on Pt(111). Instead, three different ordered structures were identified depending on the preparation conditions. The (4×4) structure is a stable structure at low oxygen concentration. This structure was formed reproducibly after exposing any of the surfaces discussed here with a saturation dose of NO_2 and subsequent annealing. For the oxi-

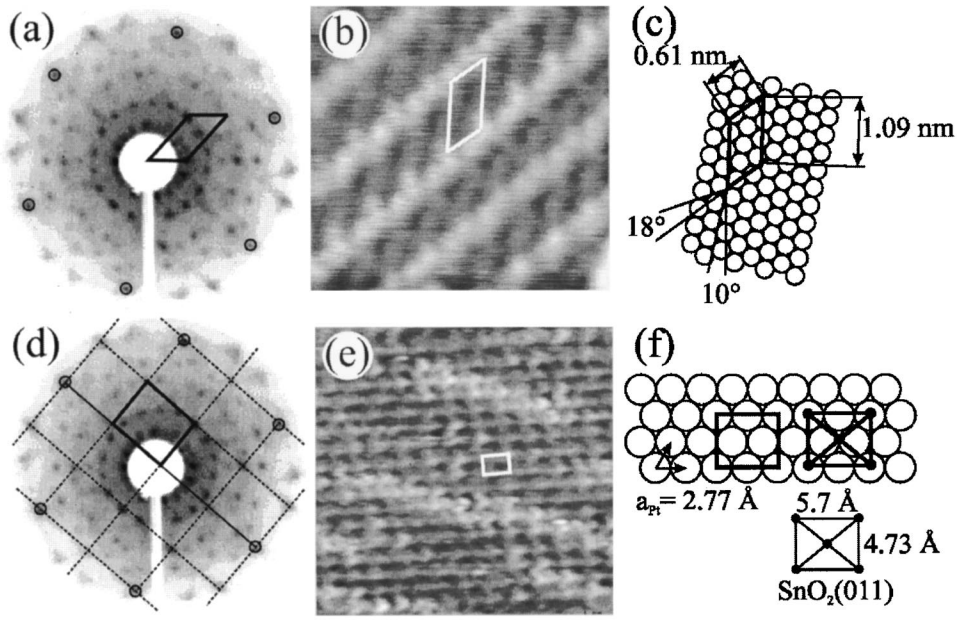

FIG. 5. Structural analysis of a Sn oxide overlayer on Pt(111) responsible for structure II. (a) LEED pattern in which a unit cell is indicated. The first-order Pt(111) spots are marked by circles (E_p=77 eV). (b) STM image (U_{bias}=200 mV, I=0.2 nA) of structure II on the surface, along with the same unit cell that was derived from LEED. (c) Models showing dimensions and orientation of the unit cell with respect to the Pt(111) lattice. (d) Same LEED pattern as in (a) in which a rectangular coincidence cell with Pt(111) lattice is indicated. This rectangular cell cannot always be identified with structure II, and appears to be present only if STM images indicate a high defect density. (e) STM image (U_{bias}=100 mV, I=0.4 nA) that shows rectangular unit cells in a region of the surface that possesses a ''fragmented'' row structure. (f) A square unit cell is indicated on top of the Pt(111) lattice. The size of this cell is very similar to the unit cell of the rutile SnO_2(011) face. This unit cell, showing the position of the Sn atoms, and its dimensions are provided for comparison.

dized $(\sqrt{3}\times\sqrt{3})R30°$ alloy, another structure denoted as structure I formed over a narrow temperature regime. Replacement of structure I by the (4×4) structure upon annealing to 850 K for a prolonged time or flash annealing to higher temperatures coincides with a small increase in the metallic tin component in XPS spectra as reported previously.[37] This was explained by Sn segregation from the bulk to the surface. TPD studies[38] and the AES data of Fig. 1 establish that no oxygen is lost in the temperature regime in which the transition from structure I to the (4×4) structure takes place. Thus, the only change is the increased tin content in the surface region due to a small amount of tin segregation, and this is responsible for the structural change. This interpretation is further supported by the fact that repeated dosing of NO_2 on the (4×4) structure results in a surface covered by structure I that is stable and does not transform into a (4×4) structure upon annealing. The stability of structure I after the second NO_2 exposure can be explained by the lack of sufficient subsurface tin after the second oxidation and annealing cycle to segregate to the surface. Thus, tin segregation to the surface is responsible for the formation of the (4×4) structure after annealing the oxidized $(\sqrt{3}\times\sqrt{3})R30°$ alloy. We speculate that tin segregation results in the formation of a (2×2) Sn/Pt(111) surface alloy at the interface between the Pt single crystal and the tin oxide layer. This change at the interface, from a Sn oxide adlayer on a Pt(111) surface to a Sn oxide adlayer on a (2×2) Sn/Pt(111) alloy, may trigger the restructuring of the oxide film into a (4×4) structure. The coincidence structure of the (4×4) structure of the SnO_x adlayer with the (2×2) Sn/Pt(111) surface alloy supports this proposal. Such a periodic coincidence lattice is commonly observed for the adsorption of molecules on surfaces, and this suggests that the observed (4×4) adlayer consists of single Sn_xO_y pseudomolecules with preferential adsorption sites on the surface. STM images support such an interpretation.

One may expect that if a (2×2) alloy interfacial structure is necessary to form the (4×4) oxide overlayer structure, then such an oxide structure should also form if we start with a (2×2) Sn-Pt surface alloy. However, as was mentioned in the Introduction, such an ordered oxide is not observed for the oxidation of a (2×2) surface alloy. This is no contradiction, since after oxidation of the Sn in the (2×2) alloy there is not enough Sn left in the substrate to reform the alloy interface. Indeed, this lack of metallic Sn in the substrate may be the origin for the reduced thermal stability of the oxide films obtained by oxidation of a (2×2) surface alloy.

Oxidation of a 0.4-ML Sn overlayer using NO_2 and following the same procedures also results in the formation of a (4×4) structure. If a (2×2) interface alloy is necessary to form the (4×4)-oxide coincidence structure, then some alloying of Sn with Pt has to occur. This can only happen if some of the initially disordered, Sn oxide overlayer partially decomposes to release enough tin from the oxide film to form an alloy during annealing. It is likely that Pt facilitates the partial decomposition of the Sn oxide overlayer in a manner that is similar to that previously suggested for Sn oxide

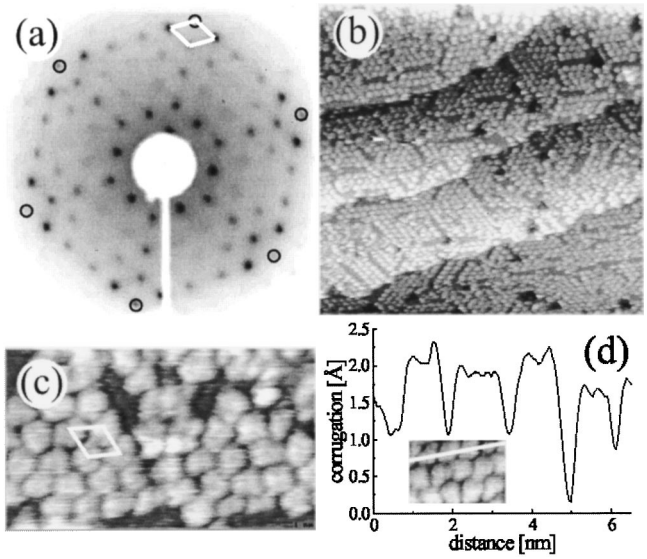

FIG. 6. The (5×5) Sn oxide overlayer on Pt(111) that was obtained by repeatedly oxidizing and annealing a Sn/Pt surface alloy. (a) (5×5) LEED pattern with the unit cell indicated. The first-order diffraction spots of the Pt(111) substrate are marked by circles ($E_p=75$ eV). (b) Large-area scan STM image (62×62 nm^2, $U_{\text{bias}}=500$ mV, $I=0.4$ nA) showing atomic steps similar to those observed on clean Pt(111) surfaces. A regular array of Sn oxide islands are imaged on top of the terraces. (c) Small-scan STM image showing an ordered Sn oxide island structure with the islands arranged on a (5×5) grid as indicated by the superimposed unit cell. (d) Cross section along the line indicated in the inset. The island corrugation is about 2 Å.

films on Pd(111).[15] We propose that once a (2×2) interface alloy is formed, the remaining Sn oxide adlayer is stable and can form the ordered (4×4) overlayer structure. In such a scenario, 0.25 ML of Sn is lost from the initial 0.4-ML Sn overlayer to form the (2×2) interface alloy, leaving 0.15 ML of Sn to form the (4×4) Sn oxide adlayer.

A second oxidation cycle applied to the (4×4) surface, obtained either by oxidizing and annealing the $(\sqrt{3}\times\sqrt{3})R30°$ alloy or a 0.4-ML Sn adlayer, results in the formation of structure I on the surface. This treatment increased the O(510 eV)/Sn(430 eV) ratio in AES by a factor of 1.4 and the O(510 eV)/Pt(237 eV) ratio by a factor of 1.6 compared to those values before the second cycle. This indicates that structure I is more oxygen rich than the (4×4) surface structure. The increase in oxygen concentration can be explained by oxidation and extraction of part of the Sn in the (2×2) Sn/Pt(111) alloy at the interface. Extraction of Sn out of an interface Sn/Pt alloy into a Sn oxide overlayer is consistent with the attenuation of the Pt AES signal and associated larger increase in the O/Pt ratio compared to the O/Sn ratio. In the following, we propose and discuss possible real space structural models for the different surface morphologies.

A. The (4×4) structure

The unit cell of the (4×4) structure is easily determined from LEED and STM. It can be constructed from the protrusions visible in the STM images with a separation of twice the Pt(111) surface lattice constant, with every second protrusion missing in every second row. The ''missing'' protrusions define the (4×4) unit cell shown in Figs. 3(c) and 3(d). The large corrugation of the protrusions (0.1 nm) observed by STM implies that these protrusions have a topographical origin and are not just due to electronic effects. Because the protrusions form a coincidence lattice with Pt(111) and the (2×2) Sn/Pt(111) surface alloy, as is observed commonly for the adsorption of molecules on surfaces, we propose a model where the protrusions consist of Sn_xO_y ''molecules'' populating preferred substrate sites. There is precedence for such a proposal. Such pseudomolecules are formed upon oxidation of one-component, single-crystal metal surfaces. These pseudomolecules usually order into metal-oxygen ''chains'' along low-index crystallographic directions.[42–45]

An upper limit for the amount of Sn atoms can be established in this particular Sn oxide adlayer by assuming that all of the Sn in a $(\sqrt{3}\times\sqrt{3})R30°$ surface alloy was oxidized and extracted into the adlayer after the first oxidation step. This amounts to $\Theta_{\text{Sn}}=0.33$ in the disordered oxide adlayer. The primitive unit cell of the (4×4) structure, on the other hand, corresponds to a coverage of $\Theta=0.19$ for Sn_xO_y molecules at the surface. Therefore, retention of all of the Sn in the disordered adlayer to form the ordered adlayer provides an upper limit of about two Sn atoms per pseudomolecule. This stoichiometry would also come about if the (4×4) structure exists on essentially a (1×1)Pt(111) surface layer. The actual stoichiometry may be lower depending on how much tin is consumed to reform a (2×2) interface alloy from the preexisting disordered oxide overlayer and/or structure I on the surface. Although previous XPS studies[37] showed that some tin segregates from subsurface regions to the interface, this may not be enough to form the (2×2) interface alloy and then some tin would be lost from the oxide overlayer. If the stoichiometry was only one Sn atom per pseudomolecule, then about 0.14 ML of the Sn required to form the (2×2) alloy came from reduction of the preexisting oxide adlayer. We favor a stoichiometry of one Sn atom per molecule because formation of the (4×4) structure from an oxidized 0.4-ML Sn *overlayer* leaves only $\Theta_{\text{Sn}}=0.15$ in the Sn oxide adlayer after forming the (2×2) interface alloy.

Previous TPD studies determined that the oxygen coverage for the (4×4) structure is about 0.15 ML.[38] This indicates that there is only one oxygen atom per pseudomolecule. These considerations lead to the conclusion that each protrusion in the STM image consists of one SnO pseudomolecule. The two-dimensional arrangement of these pseudomolecules is shown in Fig. 3(d), assuming a particular registry with the substrate, but obviously the identity of adsorption sites for these molecules is not known.

B. Structure I and the (5×5)-island structure

Some obvious similarities between structure I and the (5×5)-island structure, in addition to the fact that the latter structure evolves from the former one, suggest that both of these structures are closely related. The similarities are that

the LEED pattern of structure I contains (5×5) spots and that STM reveals rows in the images of structure I that have the same separation as the islands in the (5×5) structure. Furthermore, the hexagonal island structure is characterized by ''rows'' of islands along the same directions as those for the three domains of rows of structure I. The transition from structure I to the (5×5)-island structure occurs following repeated NO_2 dosing and annealing. This implies that the island structure is either more fully oxidized or more tin is extracted from the Sn/Pt alloy to form the oxide adlayer than in the case for structure I. The O(510 eV)/Sn(430 eV) AES ratio, however, increases only slightly from 0.40 to 0.42, implying that only a small amount of additional oxygen is necessary to have this profound effect. We propose that these islands form to relieve stress in the tin oxide adlayer. If island formation is driven by stress relief in the adlayer, then the rows in structure I are likely to be associated with a stress-relief pattern, too. While a few of the spots in the LEED pattern of structure I can be associated with the row pattern in the STM images, there are additional spots that are unaccounted for and that cannot be found in the (5×5) island structure. It is interesting to note that some of these spots can be constructed easily by rotating the (5×5) unit cell by 30°. This may indicate the existence of other domains rotated by 30°. Another dominant feature in the LEED pattern are diffuse spots in the low-index directions. These spots correspond to a lattice vector of 1.6 times the surface lattice vector of the Pt(111) substrate. These diffuse spots may indicate some ordering in the adlayer beyond the rowlike pattern. Although the length of this vector is not an integer multiple of the Pt substrate, the direction of this vector along the low-index direction of the substrate indicates that the overlayer is strongly influenced by the Pt substrate and there must exist strong interactions between the tin oxide adlayer and the Pt substrate. The diffuseness of the LEED spots indicates that there is only weak order in the adlayer. No such spots are present in the LEED pattern of the (5×5)-island structure. We propose that the increased adlayer coverage for the (5×5)-island structure compared to structure I increases the stress in the adlayer and causes the film to form an array of islands as a mechanism to reduce the strain energy. In the LEED pattern of the island arrays, only (5×5) spots were seen. These spots are entirely due to the organization of the islands on the Pt(111) surface in a (5×5) grid, and thus the individual islands do not show any long-range coherence of possible internal structure that extends over several islands. Also STM images do not show any order within the islands and the islands are imaged with no regular shape.

STM images of structure I only show small corrugations. From the STM data alone, it is not possible to conclude whether the observed features are topographic or electronic in origin. For instance, antiphase boundaries in Al_2O_3 thin films are often imaged as protruding in STM, although atomic force microscopy (AFM) shows that they are depressions.[46] On the other hand, the (5×5) island structure exhibits a corrugation for the ''trenches'' between the islands of 0.2 nm, which is close to the topographical value one would expect for a one-monolayer-thick island.

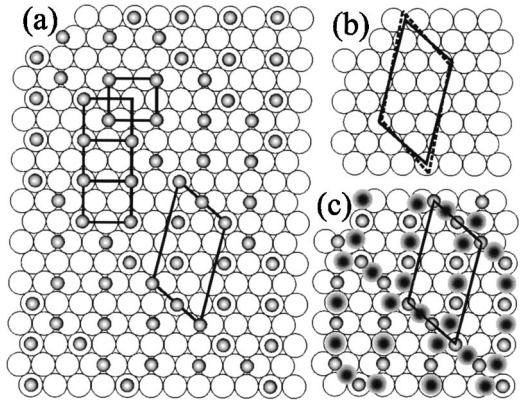

FIG. 7. Proposed structural model for a structure II–type Sn oxide overlayer. (a) The shaded circles indicate Sn atoms on a Pt(111) (open circles) substrate. The rectangular ''building blocks'' are of the same size as the rectangles observed in STM images at defect sites of structure II and correspond to coincidence spots found in LEED for these surfaces [see Figs. 5(d)–5(f)]. Every third rectangle is shifted to form a face-centered structure. This arrangement of rectangles results in the large unit cell indicated at the right. The Sn coverage in this model corresponds to $\frac{1}{3}$ of a monolayer. (b) The unit cell of the model in (a) (solid line) is compared with the unit cell deduced from LEED (dashed line). There is only a small discrepancy between the two unit cells. (c) Same model as (a) with possible positions of the oxygen atoms indicated corresponding to an ultrathin film of SnO.

C. Structure II

Structure II shows clear features in STM images and LEED. The complex LEED pattern and long-range Moiré pattern observed in STM images indicates that this surface is incommensurate with the Pt(111) substrate. The decoration of these domains with ''material'' indicates that these SnO_x monolayers can only accommodate a fixed amount of Sn and excess Sn diffuses to the domain boundaries. The fact that only structure II domains are decorated and not structure I domains is consistent with the impression that structure II is better ordered and exists only for a well-defined Sn coverage. The unit cell that can be constructed from the LEED and STM images was shown in Fig. 5(c). In our attempts to account for this unit cell, we noted the intriguing feature that there are commensurate $\left(\begin{smallmatrix}2 & 0\\ 1 & 2\end{smallmatrix}\right)$ unit cells in incompletely ordered overlayers, i.e., overlayers that had a high defect density in the rows of structure II. The size of this unit cell matches very closely the unit cell of a rutile $SnO_2(011)$ face as shown in Fig. 5(f). This suggests a structural relationship between the $SnO_2(011)$ face and the Sn oxide overlayer on Pt(111) denoted as structure II. In Fig. 7(a), a model is drawn with a unit cell that is very close to the measured unit cell that was shown in Fig. 5(c). In this model, a structure is constructed that essentially consists of rectangular cells with a $\left(\begin{smallmatrix}2 & 0\\ \bar{1} & 2\end{smallmatrix}\right)$ geometry. Every third cell in the $\langle 211\rangle$ direction of the Pt(111) substrate is shifted such that the corner of the cell now lies in the center of an unshifted cell, creating a cell with a centered atom. The unit cell of such a structure can be expressed in matrix notation as $\left(\begin{smallmatrix}3 & \bar{2}\\ 1.5 & 5\end{smallmatrix}\right)$.

The unit cell of this model is compared directly with that deduced from LEED and STM measurements in Fig. 7(b). Although the two unit cells do not match perfectly, they have a similar size and orientation with respect to the Pt(111) substrate. The close match of the two unit cells and other structural features of the model and STM images, i.e., the row structure and the connecting ''pegs'' between the rows that give the structure a ''skewed ladder'' appearance, supports our proposed model for structure II. Furthermore, the proposed overlayer model was drawn with $\Theta_{Sn}=0.33$, which is exactly the amount of Sn available from the $(\sqrt{3}\times\sqrt{3})R30°$ Sn/Pt surface alloy. The small discrepancy between the measured unit cell and that of the proposed model is not surprising because it is known from the observed Moiré pattern that the overlayer is incommensurate with the Pt lattice, and this is not explained by this simple model. Competition between the occupation of preferential sites on the Pt(111) substrate by atoms in the overlayer and formation of preferred interatomic bond distances within the overlayer would expectedly lead to some stretching and/or skewing of the structure of this proposed model to form the observed structure.

No information about the position of the oxygen atoms in the tin oxide film are available. However, the separation between the Sn atoms in the model is reasonable to form Sn-O bonds because of the similarity that the rectangular $\left(\begin{smallmatrix}2 & 0\\ 1 & 2\end{smallmatrix}\right)$ ''building blocks'' have to the rutile $SnO_2(011)$ surface. In Fig. 7(c), possible locations for the oxygen atoms in our model are included assuming a stoichiometry of SnO. Evidence for this comes from AES data. AES shows an increase in the O(510 eV)/Sn(430 eV) ratio by a factor of 1.4 compared to the (4×4) structure. This occurs because the additional oxygen uptake in the second oxidation step extracts Sn that was alloyed in the (4×4) structure to increase the amount of oxidized Sn in the adlayer from 0.19 ML of SnO pseudomolecules in the (4×4) structure to 0.33 ML of SnO in structure II.

The increased oxygen concentration along the rows that is suggested in Fig. 7(c) is also consistent with the contrast reversal that is observed in STM upon pickup of an adsorbate by the tip [Fig. 4(d)]. For instance, a stronger interaction of the ''tip'' with the more reduced areas of the surface can be anticipated if an oxygen atom is attached to the apex of the STM tip, and this would result in an increased apparent corrugation of these parts in the STM image.

V. CONCLUDING REMARKS

There are many systems where there is a strong dependence of the structure of an ultrathin oxide film on the preparation conditions. In particular, it has been observed frequently that there is a transition from a disordered, amorphous oxide film to an ordered overlayer with increasing substrate temperatures. For this particular system of ultrathin tin oxide films on Pt(111), we showed that a variety of structures can form, which should possess different and potentially unique physical and chemical properties. Tin oxide films that form an ordered stress-relief pattern and evolve into an ordered tin oxide island array after further oxidation steps have been identified. This array of islands exhibits a lateral superlattice with a (5×5) periodicity with respect to the Pt(111) substrate.

Two ordered, tin oxide adlayers were observed. One structure formed a (4×4) coincidence lattice with the Pt(111) substrate, resembling structures commonly observed for molecular adsorption on surfaces. Consequently, we concluded that SnO pseudomolecules form on these surfaces with preferential adsorption sites. The other ordered tin oxide overlayer formed an incommensurate structure.

Slight variations in the amount of tin and oxygen in the oxide layer, as well as alloying of Sn with the Pt(111) substrate at the interface, control important aspects of the formation of the different oxide structures. Thus, subtle variations of the preparation conditions may result in different stable and metastable surface structures for tin oxide adlayers on Pt(111) and Pt-Sn alloys.

Repeated oxidation and annealing were used to alter the oxide-film morphology. This was possible even though the first oxygen exposure consisted of a saturation dose and most of the oxygen desorbs at an annealing temperature below the onset of ordering of the oxide films. Repeated oxidation changes the tin to oxygen stoichiometry only minutely but has a profound effect on the structure of the oxide film. We are not aware of any similar studies that employed cycles of oxidation and annealing to form ultrathin oxide overlayers. This may, however, be an important technique for the fabrication of unique oxide-overlayer structures.

Even after repeated oxidation under these conditions, no film with SnO_2 stoichiometry was formed. Although SnO_2 is the most stable oxide of tin in bulk material, only a more reduced tin oxide compound is thermodynamically stable at the Pt/tin oxide interface.

In this study, we demonstrated that subtle differences in the preparation of ultrathin oxide films can produce surfaces with different structures and potentially different properties. This illustrates the complexity of such interfaces and the challenge this presents to tackling these interfaces using theoretical methods. This also illustrates the difficulties that may be encountered in the controlled preparation of such metal/oxide interfaces. However, the variety of oxide/metal structures that can be formed illustrates the potential for engineering novel materials and interfaces at the nanoscale level.

ACKNOWLEDGMENTS

This work was partially supported by the Analytical and Surface Chemistry Program in the Division of Chemistry, National Science Foundation (NSF). One of the authors (M.B.) gratefully acknowledges financial support from the Deutsche Forschungsgemeinschaft (DFG).

*Corresponding author. Electronic mail address: koel@chem1.usc.edu

[1] S. C. Street, C. Xu, and D. W. Goodman, Annu. Rev. Phys. Chem. **48**, 43 (1997).
[2] S. A. Chambers, Surf. Sci. Rep. **39**, 105 (2000).
[3] H.-J. Freund, Faraday Discuss. **114**, 1 (1999).
[4] C. T. Campbell, Surf. Sci. Rep. **27**, 1 (1997).
[5] D. W. Goodman, Surf. Rev. Lett. **2**, 9 (1995).
[6] H.-J. Freund, Angew. Chem. Int. Ed. Engl. **36**, 452 (1997).
[7] C. R. Henry, Surf. Sci. Rep. **31**, 231 (1998).
[8] C. Xu and D. W. Goodman, Chem. Phys. Lett. **263**, 13 (1996).
[9] D. R. Rainer and D. W. Goodman, J. Mol. Catal. A: Chem. **131**, 259 (1998).
[10] H. C. Galloway, J. J. Benitez, and M. Salmeron, Surf. Sci. **298**, 127 (1993).
[11] H. C. Galloway, J. J. Benitez, and M. Salmeron, J. Vac. Sci. Technol. A **12**, 2302 (1994).
[12] H. C. Galloway, P. Sautet, and M. Salmeron, Phys. Rev. B **54**, R11 145 (1996).
[13] M. Ritter, W. Ranke, and W. Weiss, Phys. Rev. B **57**, 7240 (1998).
[14] W. Ranke, M. Ritter, and W. Weiss, Phys. Rev. B **60**, 1527 (1999).
[15] A. F. Lee and R. M. Lambert, Phys. Rev. B **58**, 4156 (1998).
[16] K. Wilson, A. F. Lee, C. Hardacre, and R. M. Lambert, J. Phys. Chem. B **102**, 1736 (1998).
[17] P. S. Robbert, H. Geisler, C. A. Ventrice, Jr., J. van Ek, S. Chaturvedi, J. A. Rodriguez, M. Kuhn, and U. Diebold, J. Vac. Sci. Technol. A **16**, 990 (1998).
[18] C. A. Ventrice, Jr., T. Bertrams, H. Hannemann, A. Brodde, and H. Neddermeyer, Phys. Rev. B **49**, 5773 (1994).
[19] K. D. Schierbaum, Surf. Sci. **399**, 29 (1998).
[20] L. Zhang, M. Kuhn, and U. Diebold, Surf. Sci. **375**, 1 (1997).
[21] Y. Zhang and A. J. Slavin, Phys. Rev. B **49**, 2005 (1994).
[22] A. F. Lee, C. J. Baddeley, M. S. Tikhov, and R. M. Lambert, Surf. Sci. **373**, 195 (1997).
[23] R. D. Cortright and J. A. Dumesic, J. Catal. **157**, 576 (1995).
[24] G. B. Hoflund, D. A. Ashbury, and R. E. Gilbert, Thin Solid Films **129**, 139 (1985).
[25] F. M. Dautzenberg, J. N. Helle, P. Biloen, and W. M. H. Sachtler, J. Catal. **63**, 119 (1980).
[26] J. Voelter, G. Lietz, M. Uhlemann, and M. Hermann, J. Catal. **68**, 42 (1981).
[27] E. Marlen, P. Beccat, J. C. Bertolini, P. Delichere, N. Zanier, and B. Didillon, J. Catal. **159**, 178 (1996).
[28] Y. Zhou and S. M. Davis, Catal. Lett. **15**, 51 (1992).
[29] Y. X. Li, K. J. Klabunde, and B. H. Davis, J. Catal. **128**, 1 (1991).
[30] H. Lieske and J. Volter, J. Catal. **90**, 96 (1984).
[31] K. Balakrishnan and J. Schwank, J. Catal. **132**, 451 (1991).
[32] K. Grass and H. G. Lintz, in *Spillover and Migration of Surface Species on Catalysts*, edited by C. Li and Q. Xin (Elsevier, New York, 1997), p. 135.
[33] J. F. McAleer, P. T. Moseley, J. O. W. Norris, and D. E. Williams, J. Chem. Soc., Faraday Trans. 1 **83**, 1323 (1987).
[34] R. Sanjinés, C. Coluzza, D. Rosenfeld, F. Gozzo, P. Alméras, F. Levy, and G. Margaritondo, J. Appl. Phys. **73**, 3997 (1993).
[35] S. Semanski and R. E. Cavicchi, Thin Solid Films **206**, 81 (1991).
[36] D. F. Cox, T. B. Fryberger, and S. Semancik, Phys. Rev. B **38**, 2072 (1988).
[37] M. Batzill, D. E. Beck, D. Jerdev, and B. E. Koel, J. Vac. Sci. Technol. A **19**, 1953 (2001).
[38] N. A. Saliba, Y. L. Tsai, and B. E. Koel, J. Phys. Chem. B **103**, 1532 (1999).
[39] M. T. Paffett and R. G. Windham, Surf. Sci. **208**, 34 (1989).
[40] M. Batzill, D. E. Beck, and B. E. Koel (unpublished).
[41] M. Batzill, D. E. Beck, and B. E. Koel, Appl. Phys. Lett. **78**, 2766 (2001).
[42] L. Eierdal, F. Besenbacher, E. Laegsgaard, and I. Stensgaard, Ultramicroscopy **42–44**, 505 (1992).
[43] F. M. Chua, Y. Kuk, and P. J. Silverman, Phys. Rev. Lett. **64**, 1761 (1990).
[44] F. Jensen, F. Besenbacher, E. Laegsgaard, and I. Stensgaard, Phys. Rev. B **41**, 10 233 (1990).
[45] M. Taniguchi, K. Tanaka, T. Hashizume, and T. Sakurai, Surf. Sci. **262**, L123 (1992).
[46] M. Bäumer and H.-J. Freund, Prog. Surf. Sci. **61**, 127 (1999).